The Effect of Pressurized Hydrogen Gas on the Fatigue Properties of Welds in X52 and X70 Pipelines*

Report to

The US Department of Transportation, Pipeline and Hazardous Materials Safety Administration, James Merritt

DTPH5615X00004

By

E.S. Drexler, A.J. Slifka, D.S. Lauria, M. J. Connolly, and R.L. Amaro

September 25, 2016

Abstract

This report details the results of measurements of fatigue crack growth of welds in X52 and X70 pipeline steels, predominantly at a hydrogen gas pressure of 5.5 MPa. Data acquired at 34 MPa are included for comparison where available.

The goal of the study was to address the primary concern voiced by the ASME B31.12 committee on Hydrogen Piping and Pipelines. Specifically*, the heat-affected zones (HAZ) and the welds may behave differently in a hydrogen-gas environment from the base metals*. In order to compose a code that ensures the safety of the general public, measurement of fatigue properties of these regions must be performed. Since the weld material is either different from the base metal in composition or microstructure (or both), the committee decided that welds need to be evaluated for fatigue crack growth rate. Furthermore, since the weld metal has more varied microstructure and has higher residual stresses compared to the base metal, hydrogen may preferentially migrate to this region. This work is intended to contribute to possible modifications to the code that provide a basis for pipeline design based upon fatigue, the most likely failure mode of a pipeline.

A research plan was developed that included tests to assess the integrity of both seam (where relevant) and girth welds in pipelines, specifically in X52 and X70 steels. This work included measurements of fatigue crack growth rate in X52 and X70 welds at a load ratio of 0.5, loading frequency of 1 Hz, and hydrogen gas pressure of 5.5 MPa. Four girth welds and two seam welds were tested.

Welds and HAZs from four pipes showed hydrogen-assisted fatigue crack growth of the same order of magnitude as the base metal at hydrogen gas pressures of 5.5 MPa and 34 MPa. In general, the girth welds exhibited a lower FCGR than the base metal. Seam welds and the heat-affected zone from the girth weld of the vintage X52 pipe tended to have higher FCGRs than the base metal. The presence of untempered martensite in the HAZ associated with the vintage X52 girth weld is the likely source for the higher FCGR. Some anomalous behavior was seen in fatigue, mostly with girth welds and their associated HAZs. For a complete enough understanding of fatigue crack growth behavior to model and include in a code modification, more testing and modeling of these welds and HAZs is needed.

Keywords: ASME B31.12, Hydrogen-assisted cracking, hydrogen embrittlement, fatigue, fatigue crack growth rate, microstructure, pipeline steel.

Table of Contents

Acknowledgements

The authors thank Lou Hayden and James Merritt for their invaluable guidance, advice, and for support of this endeavor.

Executive Summary

Four sections of steel pipeline were acquired for fatigue testing in pressurized hydrogen gas. Two sections were grade API X70 (both were from the mid 2000s) and two were grade API X52 (one was ca. 1964, and one was ca. 2011). The vintage X52 pipe from 1964 and one of the X70 pipes had seen natural gas service. The modern X52 from 2011 was produced for hydrogen transportation, but the pipe section tested had never seen service. In order to assess what area of the pipeline was most susceptible to fatigue in pressurized hydrogen, all four girth welds and two seam welds were tested. One of the pipe sections of X70 was very short, comprising too little material to test the seam weld. The modern X52 pipe section had a seam weld fabricated by high-frequency electrical resistance. That weld was not tested because of the difficulty in finding the weld center and placing a machined crack with sufficient precision.

There were no consistent trends seen, and there were no cases where the FCGR of a weld or HAZ was so much higher than that of the previously tested base metal that would raise concerns. However, in general, the girth welds exhibited a lower FCGR than the base metal. Seam welds and the heat-affected zone from the girth weld of the vintage X52 pipe tended to have higher FCGRs than the base metal. The presence of untempered martensite in the HAZ associated with the vintage X52 girth weld is the likely source for the higher FCGR. These effects are discussed along with the contributions of residual stresses.

The fatigue crack growth data, chemical compositions, and tensile test data will be added to the ASME B31.12 code as a non-mandatory appendix. If additional testing at more conditions can be performed in the future on these welds, the appendix can be changed to a mandatory appendix.

Introduction

Ferritic steels are known to exhibit a loss of tensile ductility in the presence of hydrogen. However, when evaluating ferritic steels for transporting hydrogen gas, the response of the material to cyclic loading is far more important for the determination of fitness-for-service and design for safety. This is because all of the loss in ductility is encountered after the ultimate tensile strength is achieved, and pipelines operate at a safety margin well below the yield strength. With cyclic loading, however, a crack can initiate and grow at stresses a fraction of that of yield. Furthermore, pipelines experience periodic pressurization for storage and depressurization, at stresses well below the yield stress, as the gas is consumed. We believe that these pipelines will experience two to three pressurization cycles per day, similar to most fuel pipelines, which provide the conditions needed for fatigue crack growth (FCG).

A comprehensive testing program was previously conducted at NIST over the course of three years on the base metal from four pipelines [1]. Two API-5L X52 steels and two API-5L X70 steels were tested in air and in hydrogen gas pressurized to 5.5 MPa and 34 MPa, and at three cyclic loading rates, 1 Hz, 0.1 Hz, and 0.01 Hz (R=0.5). The results of the test program demonstrated that, unlike monotonic loading, there is no correlation between the material strength and the fatigue crack growth rate (FCGR) in hydrogen gas. The effect of gas pressure is substantial, the effect of cyclic loading rate in these three decades is minor, and it appears that microstructure may play a large role in the FCGR. Armed with this information, a model was developed at NIST to characterize the effects of pressure and loading rate on steels encompassing these grades [2]. This model has been accepted for incorporation into the ASME B31.12 code for Hydrogen Piping and Pipelines [3], and is intended to expand the choice of steel grades used in the design of future hydrogen pipelines.

Unless damage is inflicted from a third party, the most likely source of a flaw that can initiate into a crack is in the weld. This is because welds have large residual stresses, usually have larger surface roughness than the base metal, and sometimes have defects such as porosity, regions of low cohesive strength (lack-of-fusion), and inclusions. For this reason, the fatigue properties of the welds, as well as those of the base metal, must be characterized. There is relatively little known about the FCGR of pipeline weld materials and their associated heat-affected zones (HAZs) in the presence of hydrogen [4-8], and even less is known about them in pressurized hydrogen gas [4, 6]. All studies indicate that the FCGR of the weld material and/or HAZ is at least an order of magnitude higher in the presence of hydrogen than in air at values of the stress intensity range (ΔK) greater than 15 MPa·m^{½}.

Differences among base metal, weld metal, and HAZ tested in the presence of hydrogen are more subtle. Wang et al.[8] showed a lower FCGR for the X70 base metal than the HAZ from a submerged arc weld of two plates for the same conditions, where the specimens were subjected to saturated H_2S in solution. Thodla et al. [7] found that the girth weld exhibited more fatigue resistance than either the base metal or the HAZ acquired from X65 welded pipe when tested in an H_2S-saturated solution. Somerday [9] showed that at low values of ΔK (< 12 MPa·m^{½}), the HAZ for the X65 material had the lowest FCGR; whereas at higher values of ΔK, the FCGR for the base metal, weld, and HAZ were within the uncertainty of the measurement when testing at a hydrogen gas pressure of 21 MPa. The data of Moro et al. [4] fail to show any obvious differences among the base metal, girth weld metal, and HAZ of an X80 pipe tested in hydrogen gas pressurized to 10 MPa.

This confusion demonstrates the need for more data and a systematic approach to the problem. Are the observed differences the result of the different strengths of the materials tested (grades), their microstructures, the test conditions, the welding technique used, or some other variable?

In an effort to elucidate the issue of the comparative FCGR of base metal, weld metal, and HAZ, the National Institute of Standards and Technology (NIST) has conducted cyclic loading tests on different steels, weld techniques, and at two hydrogen gas pressures. A subsidiary goal of the test program was to obtain data at values of ΔK, when possible, between 8 MPa·m^{½} and 15 MPa·m^{½}, as hydrogen pipelines are expected to operate in this regime.

Materials

Four different pipe sections were used to investigate the FCGRs of base metal, weld metal, and the HAZ associated with the weld. Two of the pipe sections were API 5L X52, one from 1964 (referred subsequently as "X52 Vintage") and the other from 2011 (referred subsequently as "X52 Modern"). We define "modern" as pipeline steel that was manufactured in the 1990s or more recently. These steels are "clean" from the standpoint of low sulfur and phosphorous contents. Additionally, these modern steels generally contain small additions of micro-alloying elements such as niobium, vanadium, titanium and molybdenum. These elements form fine precipitates that anchor grain boundaries during thermo-mechanically controlled processing (TMCP), where grain refinement gives pipeline steels the combination of strength and toughness required for transport of fuels at high pressures[10-12]. We define "vintage" steels as those manufactured prior to the 1990s, which contain no micro-alloying elements (by intent) and have much higher carbon contents. The higher carbon content provides the primary strengthening mechanism through the formation of pearlite, but makes welding much more difficult than for modern, low-carbon pipeline steels. The other two pipe sections were API 5L X70 (referred to subsequently as "X70A," and "X70B"), both of which were manufactured about 2005. Table 1 provides the dimensions of each of the four pipe sections. The seam and girth welds, and their associated HAZs, were tested from the X52 Vintage pipe and the X70A pipe. Only the girth welds and their associated HAZs were tested from the X52 Modern pipe and the X70B pipe. This information is shown in Table 2, along with the techniques used to construct the weld (SMAW= shielded metal arc welding, GMAW = gas metal arc welding, and SAW = submerged arc welding). Other welding information is unknown for these pipes. Both seam welds are two-pass welds. The girth weld of the X52 modern steel appears to be an eight-pass weld, which includes the root and cap passes. The X52 vintage girth weld appears to be seven-pass weld, which includes the root and cap passes. The X70A girth weld appears to be a nine-pass weld, which includes the cap and root passes. The X70B girth weld appears to be a fifteen-pass weld, which includes the root and cap passes. Figure 1 shows composite images of the girth welds and their corresponding microhardness maps; Figure 2 shows the same for the two seam welds.

Table 1. Pipe dimensions.

Material	Pipe diameter, mm (in)	Wall thickness, mm
X52 vintage	914 (36)	10.6
X52 modern	508 (20)	10.6
X70A	914 (36)	18
X70B	914 (36)	22

Table 2. Materials tested for this investigation.

Pipe	Base Metal	Girth Weld	Girth Weld HAZ	Seam Weld	Seam Weld HAZ
X52 Vintage	X	X (SMAW)	X	X (SAW)	X
X52 Modern	X	X (GMAW)	X		
X70A	X	X (GMAW)	X	X (SAW)	X
X70B	X	X (GMAW)	X		

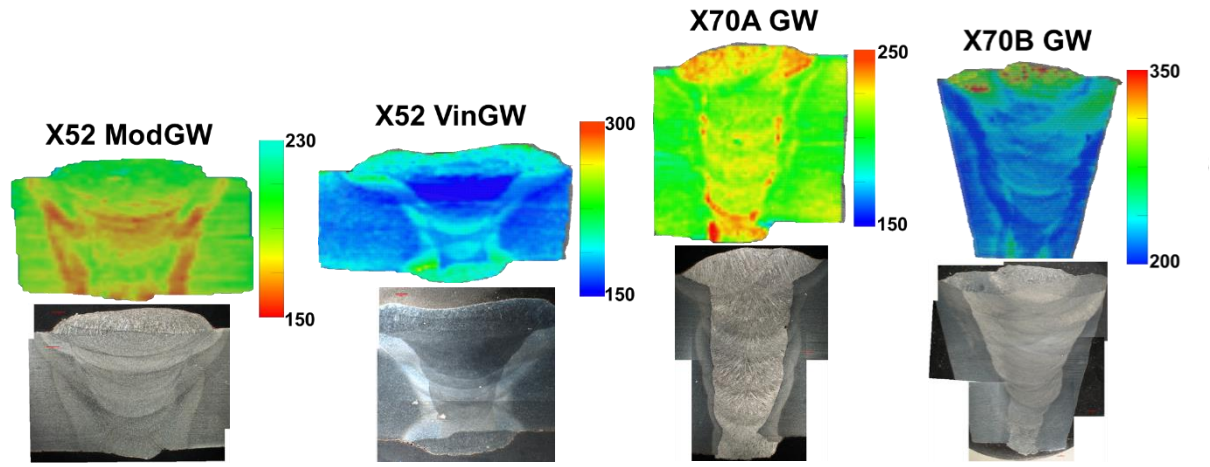

Figure 1. Microhardness maps and images of the four girth welds tested for FCGR. From left to right: Modern X52; Vintage X52; X70A; and X70B. Not shown to scale. For relative scale, recall that the X52 modern pipe is 10.6 mm thick, X52 vintage is 10.6 mm thick, X70A is 18 mm thick, and X70B is 22 mm thick. The scales are all in Vickers hardness, with the use of 0.5 kgf, which is equivalent to 4.9 newtons.

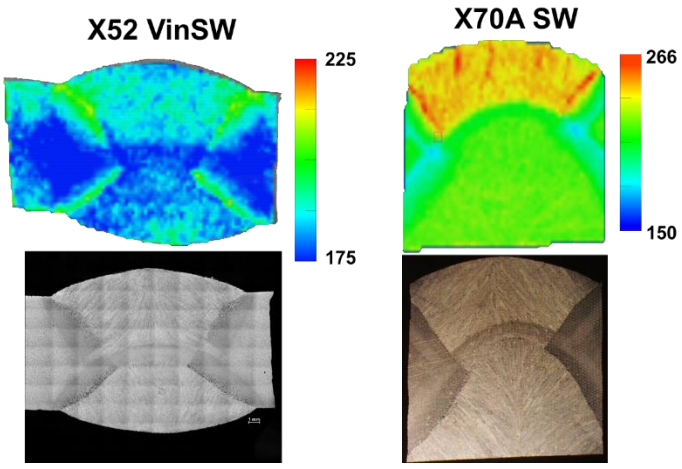

Figure 2. Microhardness maps and images of the two seam welds tested for FCGR. From left to right: Vintage X52, and X70A. Not to scale. For relative scale, the X52 vintage pipe is 10.6 mm thick, and the X70A image is 18 mm high.

The chemical composition of the base metals, determined by a commercial laboratory, can be found in Table 3, and that of the girth welds are found in Table 4. The main differences between the base metal and the corresponding weld filler material are: for the X52 vintage material there is less C and more Mo in the weld metal; there is more S, Ni, Cr, and Mo in the weld of the Modern X52 than in the base metal; there is more C and Si, and less Ni, Cr, and Ti in the weld metal of X70A than in the base metal; and there is more C, Ni, and Mo, and less Cu, Cr, and Nb in the weld metal of the X70B than in the base metal. The high C content in the base metal from the Vintage X52 pipe is indicative of when it was fabricated, as modern metallurgy lowers the C content in order to improve weldability. Interestingly, apart from the Cr content, the

compositions of the Modern X52 and X70A base metals are quite similar, although the weld metals are not.

Table 3. Bulk chemical compositions of the base metals in mass %.

Element	C	Mn	P	S	Si	Cu
X52 Vintage	0.238	0.96	0.011	0.021	0.064	0.085
X52 Modern	0.071	1.06	0.012	0.004	0.24	0.016
X70A	0.048	1.43	0.009	0.001	0.17	0.220
X70B	0.053	1.53	0.01	0.001	0.16	0.250

Element	Ni	Cr	Mo	V	Nb	Ti	Al
X52 Vintage	0.05	0.014	0.004	0.002	0.001	0.002	0.002
X52 Modern	0.016	0.033	0.003	0.004	0.026	0.038	0.017
X70A	0.14	0.240	0.005	0.004	0.054	0.027	0.015
X70B	0.14	0.230	0.003	0.004	0.054	0.024	0.012

Table 4. Bulk chemical compositions of the girth welds in mass %.

Element	C	Mn	P	S	Si	Cu
X52 Vintage GW	0.110	0.350	0.009	0.025	0.100	0.024
X52 Modern GW	0.130	0.780	0.010	0.130	0.150	0.026
X70A GW	0.087	1.360	0.010	0.009	0.730	0.200
X70B GW	0.190	0.860	0.010	0.014	0.120	0.047

Element	Ni	Cr	Mo	V	Nb	Ti	Al
X52 Vintage GW	0.046	0.018	0.430	0.006	0.001	0.005	0.010
X52 Modern GW	0.610	0.110	0.093	0.003	<0.001	0.009	0.006
X70A GW	0.059	0.043	0.002	0.003	0.010	0.002	0.012
X70B GW	0.760	0.088	0.130	0.004	<0.001	0.011	0.006

The differences in the weld chemistries were probably because the weld was designed to slightly overmatch (by strength) the grade of the base metal. However, that is not quite what occurred. Table 5 shows the tensile properties acquired in air for the base metal (BM), weld metal (GW for girth weld and SW for seam weld), and the HAZ associated with that weld (GH or SH, respectively). Tensile tests were conducted according to ASTM E-8 [13]. These pipes fall under the API 5L psl2 specification, where the yield strength, measured as a 0.5% offset, whereas the ASTM E-8 uses the 0.2 % offset, falls between 359 MPa and 531 MPa for X52, and 483 MPa and 621 MPa for X70 [14]. Table 6 shows tensile data that corresponds to the 0.5% offset from the start of the test. These yield strengths are all close, within 6 %, to those measured by way of the 0.2% offset used by ASTM. As can be seen, the Modern X52 qualifies for an X70 grade, so the strength of the GW is actually slightly undermatched to the BM. The GW from the X70B pipe was also slightly undermatched, but both the GW and SW from the vintage X52 pipe

exhibited a much higher yield strength than that of the base metal, which actually was not sufficient to qualify for the X52 grade.

Table 5. Tensile properties of the base metal (BM), girth weld (GW), seam weld (SW), Girth weld HAZ (GH), and seam weld HAZ (SH) acquired in air at room temperature.

Specimen / Property	X52 Vin BM Avg	X52 Vin GW Avg	X52 Vin GH Avg	X52 Vin SW Avg	X52 Vin SH Avg	X52 Mod BM Avg	X52 Mod GW Avg	X52 Mod GH Avg
0.2% offset YS, MPa	325	428	372	425	462	488	463	463
YP, MPa		443	371	425	455		489	469
UTS, MPa	526	520	531	549	551	588	567	526
eu	0.120	0.134	0.129	0.105	0.080	0.095	0.117	0.074
ef	0.150	0.312	0.247	0.229	0.196	0.209	0.261	0.203
E, GPa	223	193	207	199	209	215	210	198
Specimen / Property	**X70A BM Avg**	**X70A GW Avg**	**X70A GH1**	**X70A SW Avg**	**X70A SH Avg**	**X70B BM Avg**	**X70B GW AVG**	**X70B GH Avg**
0.2% offset YS, MPa	509	563	516	507	496	553	532	521
YP, MPa		575	527	516	493		570	512
UTS, MPa	609	627	603	594	603	640	616	596
eu	0.120	0.088	0.068	0.114	0.056	0.090	0.095	0.057
ef	0.297	0.263	0.233	0.294	0.205	0.274	0.260	0.187
E, GPa	221	204	194	194	212	211	208	207

In general, the HAZ materials exhibited less uniform elongation and elongation to failure than either the BM or the weld metal (WM), except for the GH from the vintage X52 pipe. Note that there was only one successful test of the X70A GH. Reported values for the base metals are the mean of three tests. Most of the welds and HAZs had only 2 tensile tests. Therefore, standard deviations are not given.

Table 6. Tensile properties comparing the 0.2 % offset yield strength to the 0.5 % offset from the start yield strength of the base metal (BM), girth weld (GW), seam weld (SW), Girth weld HAZ (GH), and seam weld HAZ (SH) acquired in air at room temperature.

	0.2% offset YS, Mpa	UTS, MPa	ef	0.5% YS, Mpa
X70A base metal	509	609	0.297	519
X70A Girth Weld	563	627	0.263	563
X70A GW HAZ	516	603	0.233	519
X70A Seam Weld	507	594	0.294	508
X70A SW HAZ	496	603	0.205	504
X70B base metal	553	640	0.274	549
X70B Girth Weld	532	616	0.260	532
X70B GW HAZ	521	596	0.187	521
X52 vintage base metal	325	526	0.150	342
X52 vintage Girth Weld	428	520	0.312	428
X52 vintage GW HAZ	372	531	0.247	385
X52 vintage Seam Weld	425	549	0.229	427
X52 vintage SW HAZ	462	551	0.196	468
X52 modern base metal	488	588	0.209	492
X52 modern Girth Weld	463	567	0.261	464
X52 modern GW HAZ	463	526	0.203	466

In addition to having similar chemistries, the microstructures of the BMs from the Modern X52 and the X70A are very similar, as can be seen in Figure 3, which shows the through-thickness microstructure of all four BMs. The X52 Vintage has a ferrite-pearlite composition and the others were determined to be polygonal ferrite and strain-induced constituents such as acicular ferrite and bainite, from optical microscopy. There may be other constituents that are not resolvable without employing more advanced analytical techniques. Microstructure images of the welds and their HAZs are shown in Figure 4.

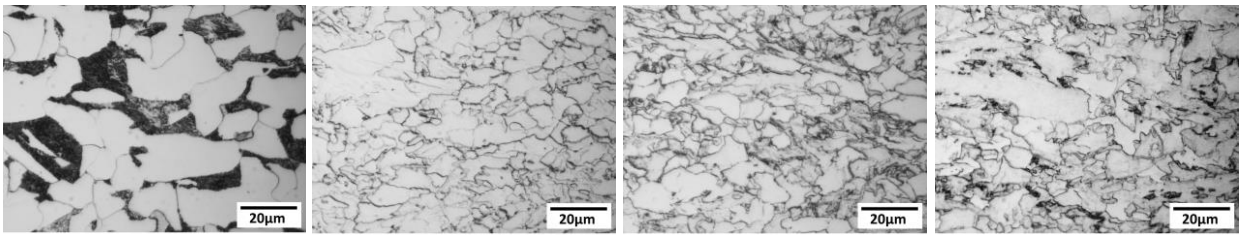

Figure 3. Microstructure images of the four base metals: Vintage X52; Modern X52; X70A; and X70B, from left to right.

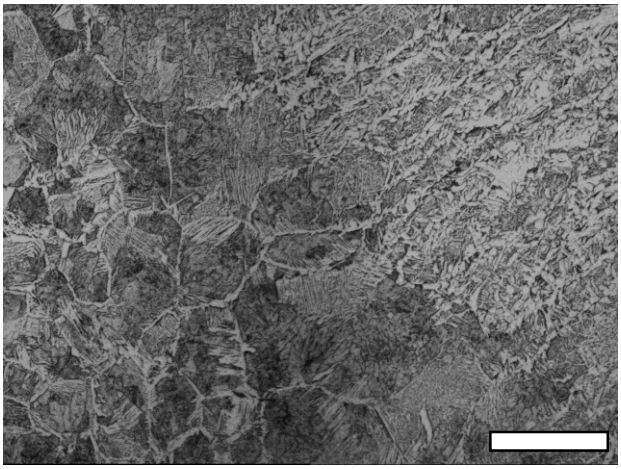

a) X52 Vintage GW

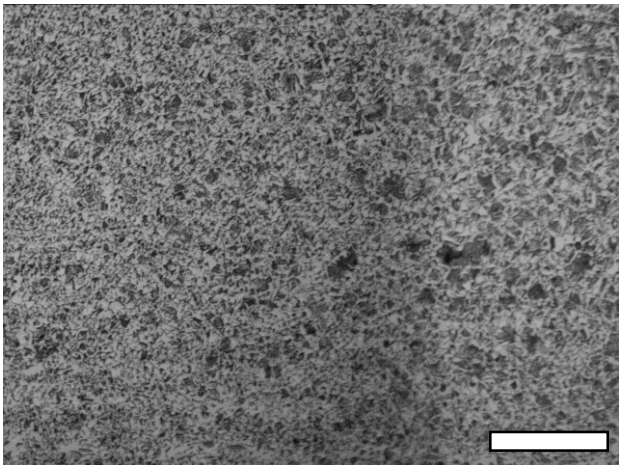

b) X52 Vintage GH

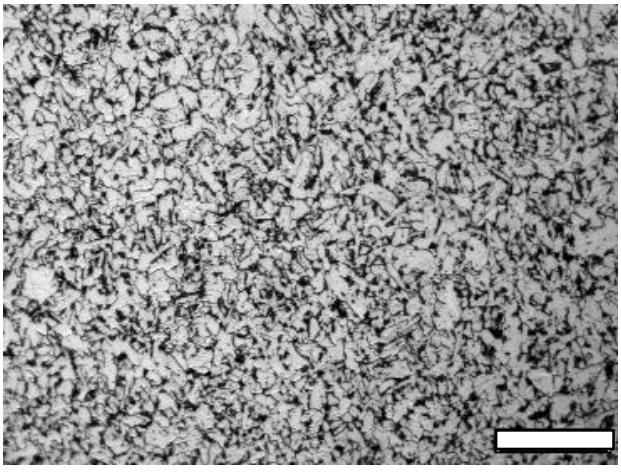

c) X52 Vintage SW

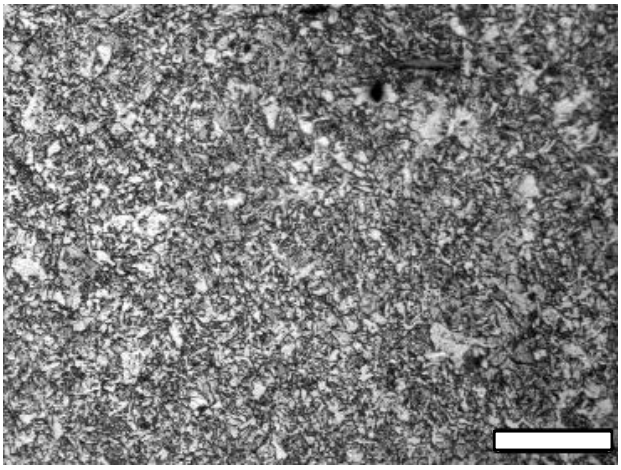

d) X52 Vintage SH

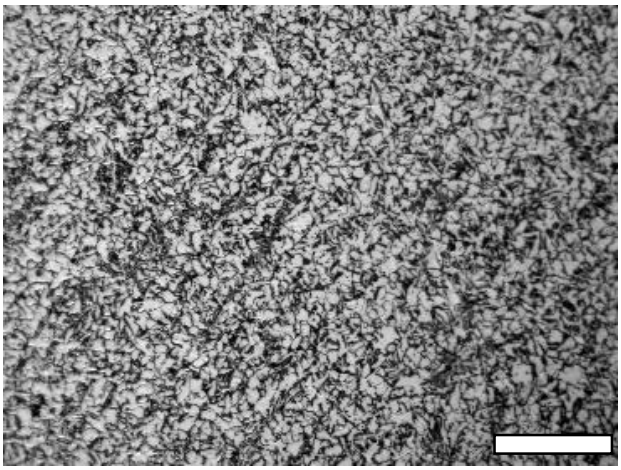

e) X52 Modern GW

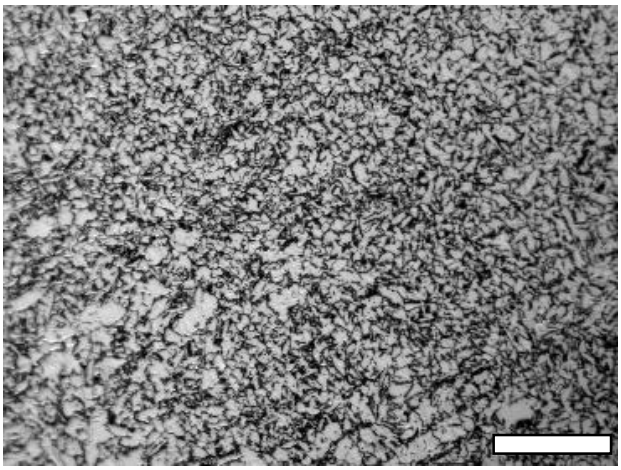

f) X52 Modern GH

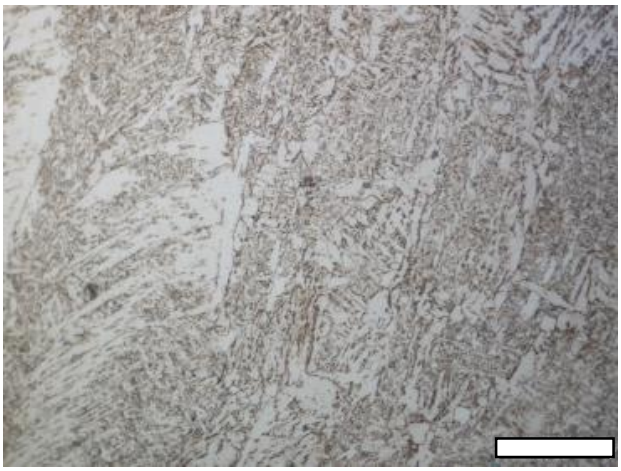

g) X70A GW

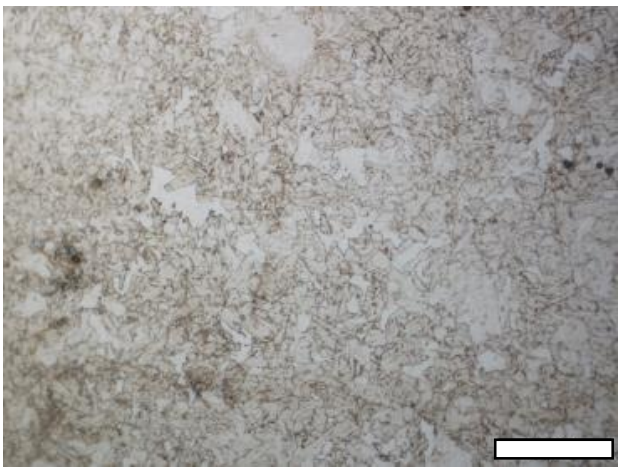

h) X70A GH

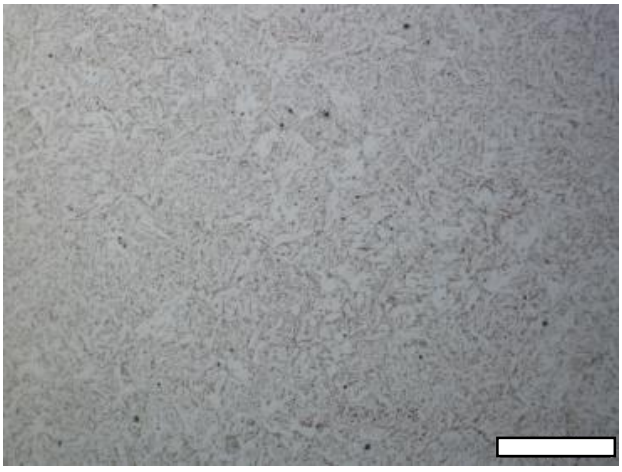

i) X70A SW

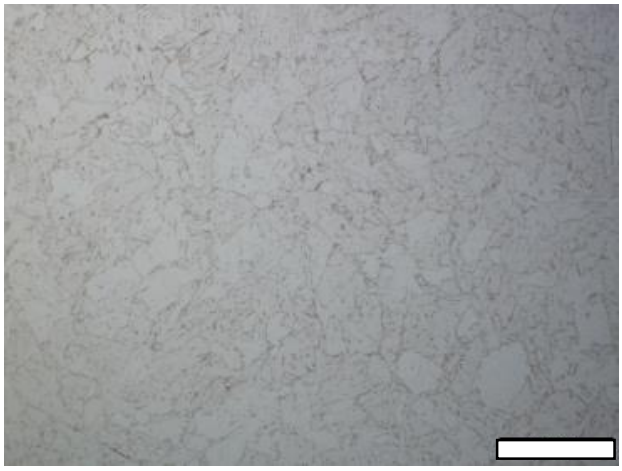

j) X70A SH

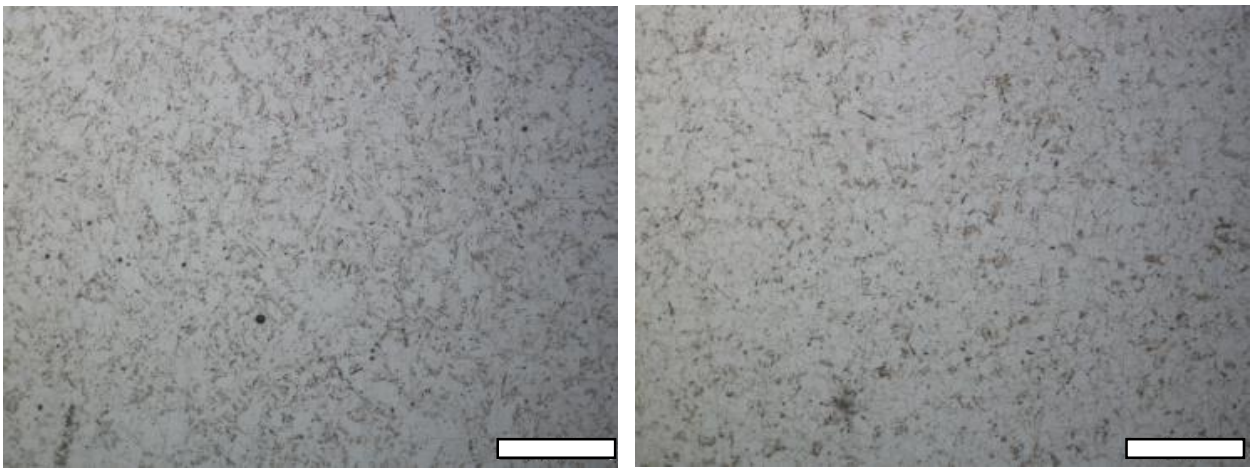

k) X70B GW **l) X70B GH**

Figure 4. Microstructure images of the welds (left) and their HAZs (right). The scale bars are 50 µm long.

Experiment

Compact-tension (CT) specimens with W=44.5 mm, where W is the specimen width, were machined in the C-L orientation for the BM, SW, and SH, and in the L-C orientation for the GW and GH specimens (Figure 5). To test the HAZ from the vintage X52, modern X52, and X70A pipe sections, the machined notched was aligned such that the midpoint of the through-thickness was at the center of the HAZ (Figure 6). The X70B material was sufficiently thick that a specimen could be machine at an angle in the through-thickness to obtain an all-HAZ notch in the specimen. Each specimen was machined with a chevron notch to facilitate initiation of the precrack and a straight crack front. The precracking was conducted at an R=0.1 in air at room temperature and at a cyclic-loading frequency of 15 Hz. A sinusoidal waveform was used. Most of the GW specimens were preloaded in compression at the crack tip to 80% of yield prior to precracking to improve crack initiation.

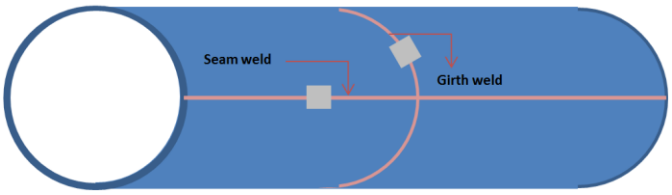

Figure 5. Schematic of the location and orientation of the weld and HAZ specimens with respect to the pipe.

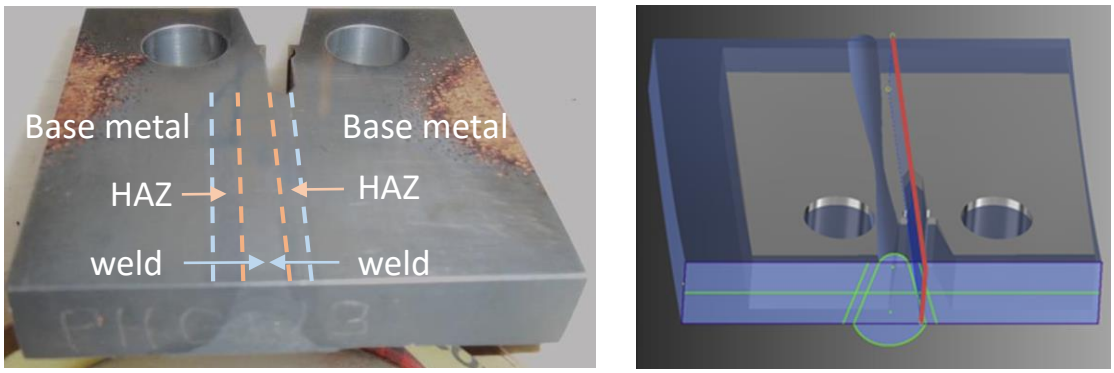

Figure 6. Machined specimen (left) and drawing of specimen (right) that show how the machined notch was aligned to test the HAZ.

Specimens were tested at an R=0.5 and a cyclic-loading frequency of 1 Hz in air or hydrogen gas that was pressurized to either 5.5 MPa or 34 MPa. Either a triangular or sinusoidal waveform was used with no discernable difference. Two test chambers, shown in Figure 7, were available for conducting cyclic-loading tests; one allowed for testing single specimens and the second allowed up to 10 specimens to be tested simultaneously. Figure 8A is a schematic of the chain of 10 specimens, and Figure 8B is a photograph of actual specimens as assembled on a table; Figure 8C shows the chain of specimens vertically mounted into the load frame with the CMOD gages in place. Details of the design of the multiple-specimen test apparatus can be found in the literature [11]. Internal load cells were employed to ensure that the forces exerted on the specimen(s) were those that were specified and were not influenced by the stiction of the seals on the chamber. Where material permitted, duplicate tests were conducted at the same condition to provide a sense of the repeatability of the data. The purging procedure and a description of the pressure-maintenance protocol can be found in [1]. Samples of each lot of the test gas were acquired and analyzed prior to use to ensure that contaminants such as oxygen and water were below 1 ppm.

(a) (b)

Figure 7. Test chambers for (a) single-specimen and (b) multiple-specimen tests.

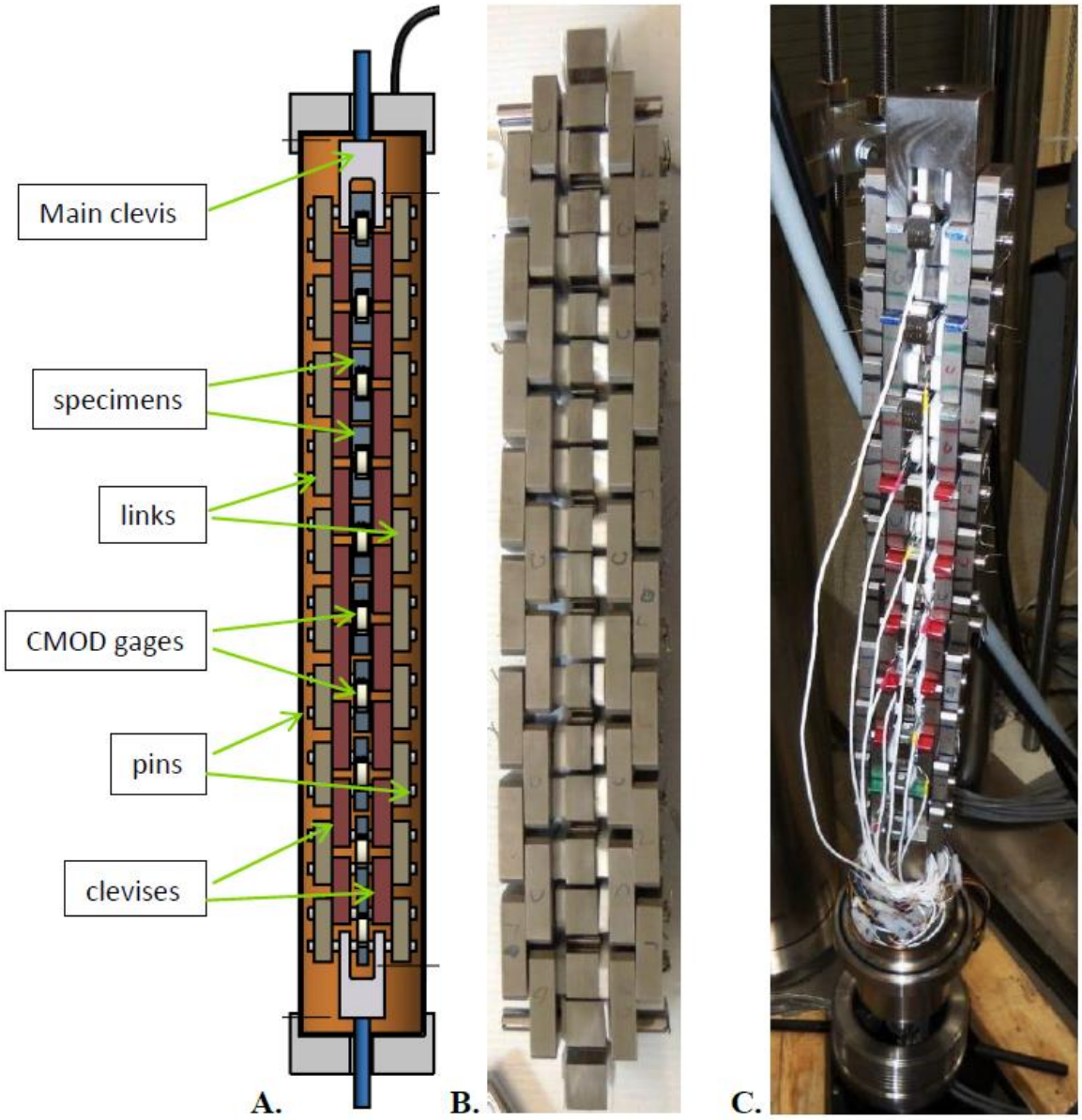

Figure 8. Conceptual drawing (A) showing the elements of the linked chain of specimens, (B) photograph showing the assembled chain with PTFE spacers, and (C) a photograph showing the assembled chain, complete with CMOD gages and aluminum spacers ready for installation in the pressure chamber.

FCGR tests were conducted according to ASTM E647 [15], and typically ran uninterrupted for weeks. Each specimen was cyclically loaded at a constant force range (rising ΔK) until a crack length (a) = 0.75 W was reached. A clip gage was attached at the load line and the crack length was calculated from compliance. Data on cycle, crack mouth opening displacement (CMOD), external force, and internal force were collected every 200 cycles for five cycles, and were used to calculate ΔK and a to generate graphs of FCGR (da/dN as a function of ΔK). Recall that a subsidiary goal of the test program was to obtain data at values of ΔK, when possible, between 8 MPa·m^{½} and 15 MPa·m^{½}, as hydrogen pipelines are expected to operate in this regime, because the crack growth rate at higher values of ΔK is so high as to be impractical for hydrogen service.

Results

Tests were conducted to compare the FCGR of base metal, weld metal, and the HAZ associated with those weld metals from four pipelines. The results of tests conducted at hydrogen gas pressurized to 5.5 MPa for each material are shown in Figure 9. The asterisk in the legend indicates a dataset that the did not meet all the validity criteria in the ASTM E647 test standard. For example, the force range did not meet the requirement of less than 2 % drift during the course of the test. Those data were included, as those tests behaved normally in other respects, and they were analyzed with the actual, not the nominal, load range. The drift was less than 4 % over a test duration of up to 10 weeks. In another case there was pinning in the precrack that affected the crack length measured from compliance, so that the effective modulus was outside the bounds of what was allowed in the standard. For those datasets, a modulus of 210 GPa was used. The BM data are shown as a single line that was visually fit to datasets from multiple tests. If shown individually, the BM data would mask the trends observed for the welds and HAZs.

Figure 9A shows the data for the FCGR tests on the vintage X52 material tested in hydrogen gas pressurized to 5.5 MPa. As with the data acquired at a hydrogen gas pressure of 34 MPa, the FCGR data from the HAZ for both the seam weld and the girth weld are higher than those of the BM. Once again, the base metal is a visual fit of datasets from multiple tests. The data from the girth weld is lower than BM at values of ΔK below 15 MPa·m^{½} and the same as the BM data above that value of ΔK. The FCGR for the weld and HAZ from modern X52 pipe (Figure 9B) fall below the BM data, although the behavior of the HAZ is unusual and needs more investigation. Both of the X70 girth welds and HAZ exhibit a reduced FCGR as compared with the BM; whereas, the X70A seam welds and HAZ are above the BM data (Figures 9C and 9D).

It can be observed that the relationship of the FCGR of the welds and HAZs to that of the base metal is not consistent from steel to steel (Figure 10). Air data (for the corresponding base metal) is shown for comparison, and is from a visual fit of multiple datasets. Similarly, the lines shown for base metals are visual fits of multiple datasets. Both the seam- and girth-weld HAZs from the vintage X52 pipe exhibited a higher FCGR than the BM, whereas the girth-weld material appeared to be more fatigue resistant than the BM at lower values of ΔK. However, the girth-weld HAZ from the modern X52 pipe exhibits a lower FCGR than the BM, and the girth weld appears to behave similarly to the BM. For the X70A material, the seam weld and its HAZ have a FCGR that is comparable to the BM; the girth-weld HAZ, however, behaves very differently. And finally, the FCGR of the girth weld and its HAZ for the X70B pipe were both similar to that

of the BM, although there was some divergence between the two girth-weld specimens. These two specimens originally were a single thick specimen that was cut in half, through the thickness, so that one characterized the inner diameter (ID) of the pipe and the other the outer diameter of the pipe (OD).

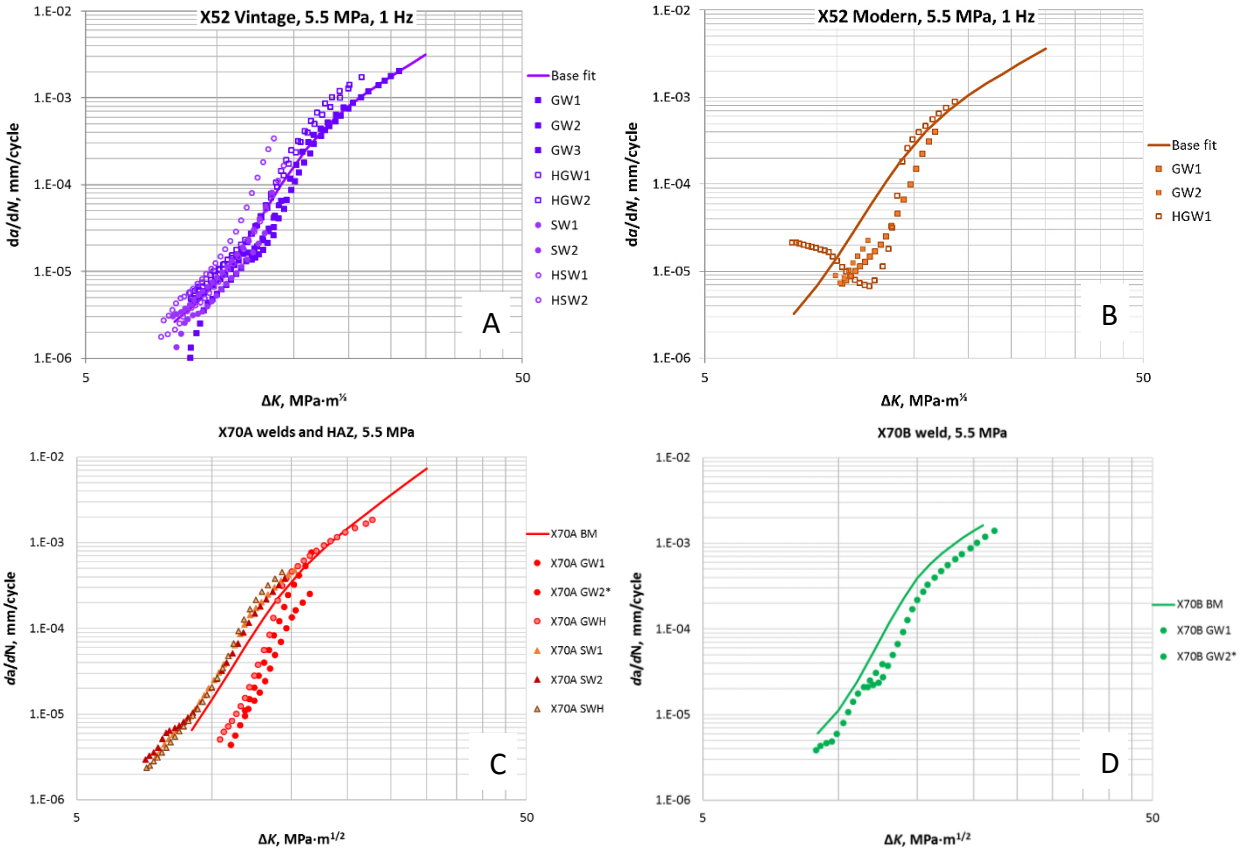

Figure 9. Data for the FCGR from tests conducted in hydrogen gas pressurized to 5.5 MPa and at a cyclic loading frequency of 1 Hz for each pipe material: (A) vintage X52, (B) modern X52, (C) X70A, and (D) X70B.

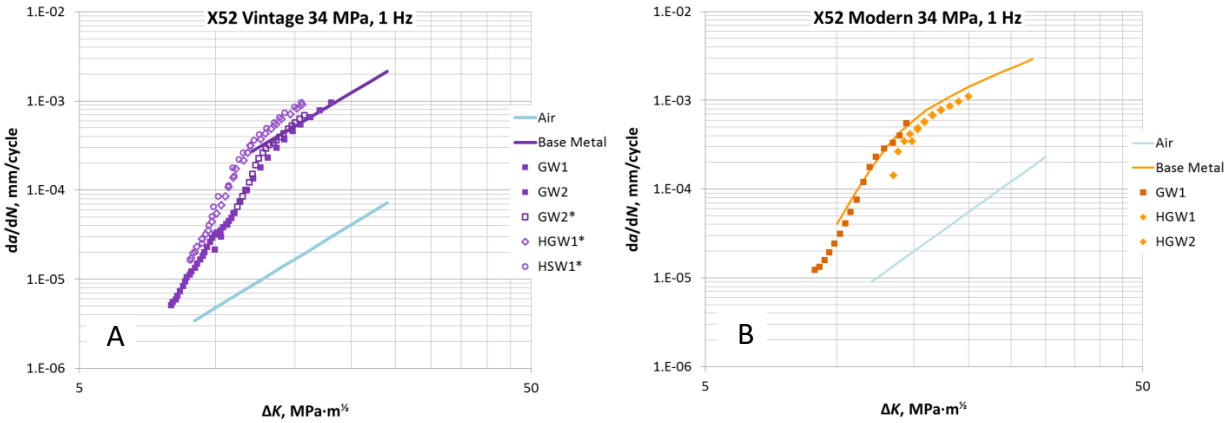

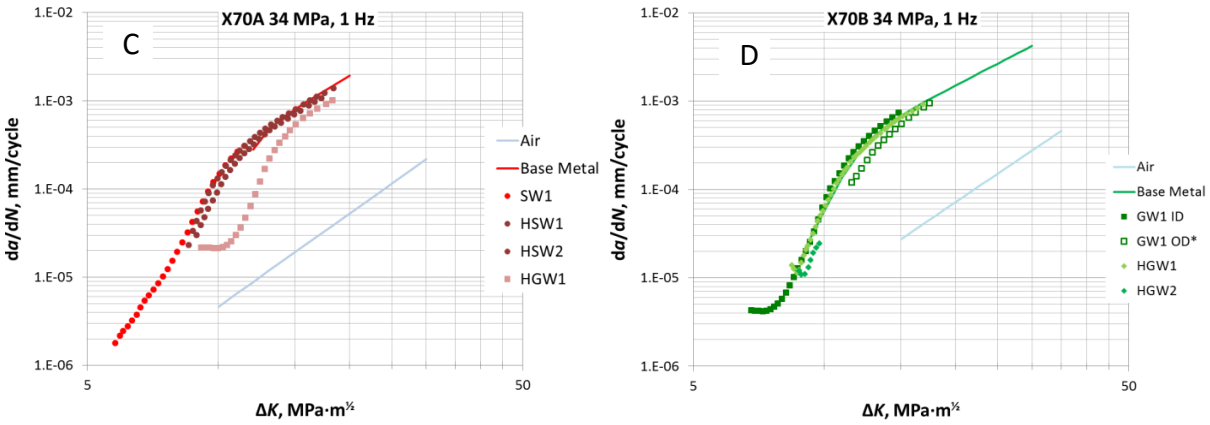

Figure 10. FCGR data from the base metal, girth weld, and HAZs associated with the seam and girth welds from the vintage X52 steel (A), the modern X52 steel (B), X70A steel (C), and X70B steel (D) tested at a hydrogen gas pressure of 34 MPa and at 1 Hz. The asterisk denotes that the measurement did not strictly adhere to ASTM E647 [12].

Several of the GW and GH specimens exhibited an unusual region at very low values of ΔK where the value of ΔK increased without an increase in the value of da/dN. The crack length with respect to number of cycles (a vs N) from these tests show a very long linear increase, such as that shown in Figure 11, followed by a rapid increase in the FCGR over a short span of ΔK.

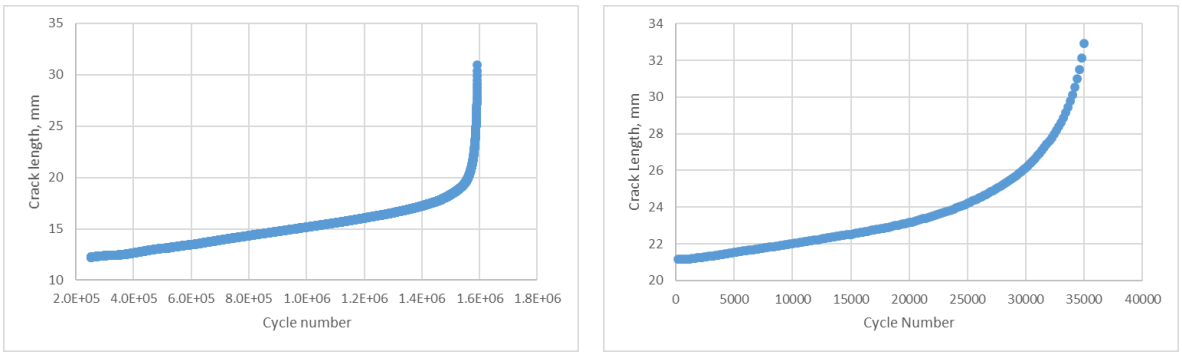

Figure 11. Crack length vs. cycles for a specimen that has a flat FCGR at the start of the test X70B ID (left) and typical FCGR from the X70B OD (right). These specimens were run in the same chain under identical conditions.

Discussion

Welds and their HAZs from ferritic pipelines experience hydrogen-assisted cracking, similar to that of the ferritic base metal. The FCGRs for all three locations in the pipe are at least an order of magnitude greater in hydrogen than those tested in air. Figure 12 shows some preliminary data from the SW and SH of the X70A pipe and the GW from the X70B pipe tested in air. Because there is little or no corrosion component to FCGR in air, there is little or no difference expected

in FCGR between welds, HAZs, and BM. If there are large enough residual stresses left in the weld or HAZ samples following machining into C(T) specimens, that could result in different FCGR behavior. The fits to the BM data tested in air and in hydrogen gas pressurized to 34 MPa are shown for comparison. Recall that the weld and HAZ tests in pressurized hydrogen were very similar to those of the BM, so this figure offers a good representation of the effect of hydrogen on the FCGR. Similar behaviors are observed whether testing is conducted at a hydrogen gas pressure of 34 MPa or 5.5 MPa.

Whether the HAZ exhibits greater FCGRs than the BM or weld appears to be inconsistent. Since the vintage and modern X52 displayed opposite behaviors, the disparity is likely attributable to one of the three main differences between the two materials: 1. the microstructure; 2. the welding technique employed; or 3. the fact that one had a significantly overmatched weld, and the other had an undermatched weld. These three items are somewhat interrelated, as the ferrite-pearlite microstructure of the vintage X52 material provided readily available C to form martensite upon heating. The combination of available C and high heat allows for formation of martensite in the HAZs of the X52 Vintage steel. Slifka et al. [16] have shown that untempered martensite was present in the HAZ of the girth weld from the vintage pipe, but not in the modern pipe. San Marchi et al. [17] found that martensite was more susceptible to hydrogen embrittlement than ferrite, the dominant constituent in the girth-weld HAZ from the modern X52 pipe, according to Slifka et al. [16].

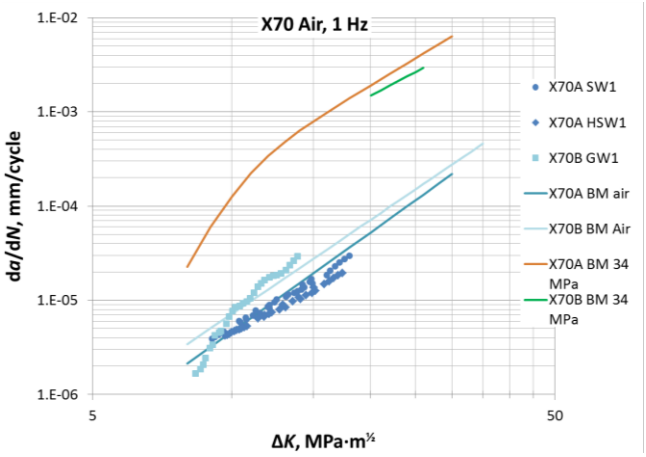

Figure 12. Preliminary FCGR data in air for the seam weld and its HAZ from the X70A pipe, and the girth weld from the X70B pipe. Data fits for the BM tested in air and at a hydrogen pressure of 34 MPa are shown for comparison.

When testing welds, residual stresses are often targeted as being responsible for anomalous behavior. However, it would be expected that when specimens this size are cut out of the pipe, residual stresses would be relieved in large part. Obvious signs of residual stresses were not observed for these tests. For example, among all those tested, nine specimens out of 22 had an uneven precrack front; all but one was associated with the girth weld. Of those, three had the shorter crack front at the ID, three had the shorter crack front at the OD, and the remainder had locations within the weld that were shorter than the rest of the crack. This inconsistency points to something other than through-thickness residual stress effects in these girth welds. Connolly et

al. [18] found that, in general, the residual stresses in these specimens of girth welds were small ($\leq$ 50 MPa) at a location 7 to 8 mm ahead of the precrack tip.

Another anomaly is that the ID of the X70B girth weld yielded a slightly higher FCGR than the OD, even though the greater hardness of the OD (Figure 1) might have indicated the opposite. As stated earlier, these two specimens (each about 10 mm thick), were originally a single specimen that was precracked as a single specimen and then sliced through the thickness. Residual stress measurements were not conducted in the through-thickness direction of the girth welds, as the welding of two unstressed bodies was not expected to be of significance through the thickness. The precrack from the ID part was about 16 % shorter than that of the OD part, which accounts for the lower starting ΔK. There were no discernable differences on the fracture surfaces of the two parts to explain the inconsistency. However, the OD section had a 4-mm difference between the crack front at one edge from the other (see Figure 13); perhaps the lagging edge impeded crack growth sufficiently to account for the difference.

Figure 13. The fracture surface of the OD of the girth weld specimen from the X70B pipe, showing the uneven precrack front.

The flat crack growth per cycle at the start of some of the girth weld tests is the final anomaly that merits discussion. It should be noted that this phenomenon occurs only in tests of the girth weld and the girth-weld HAZ. Furthermore, it was not observed in the tests from the vintage pipe. It can only be speculated that the overmatched weld provided a constraint that prevented this from occurring. Other theories have been disproved:

1. This phenomenon occurs in specimens with and without an uneven precrack.

2. It occurs in both GW and GH specimens, so it is not attributable to a tougher weld material at the edge of an HAZ specimen, which could inhibit crack growth.

3. Crack closure is unlikely with an R= 0.5, as the specimen experiences a substantial tensile force at all times.

4. Some specimens experienced uneven crack growth during the test, which was recognized by a boomerang shaped curve of Force vs. CMOD (one edge of the CMOD gage was opening more than the other). This behavior did not correlate to those specimens with the stagnant rate of crack growth per cycle.

5. No obvious differences in the fracture surface were observed in the stagnant region and the rapid regions of crack growth (See Figure 14). El-Soudani and Pelloux [19] reported on a similar flat crack-growth rate in an HAZ specimen associated with a butt weld of two aluminum plates. In their case, they were able to attribute the behavior to substantial out-of-plane deviations in the fracture surface, which they attribute to residual shear stresses at the mid thickness.

However, there is one clue from the neutron beam experiments, which were conducted to measure the residual stresses in the CT weld specimens [18]. Immediately ahead of the precrack tip, it was found that there was a compressive residual stress perpendicular and parallel to the direction of crack growth in the X70A girth weld; there was no such compressive stress in the

vintage X52 girth weld (Figure 15). The modern X52 and X70B girth welds did not show similar compressive forces, but some specimen-to-specimen variation would be expected, because of the precrack length and weld anisotropies. The magnitudes of the maximum values of residual stress might appear large in these cases. However, residual stress values below 250 MPa result in less than 4 % change in lifetime due to fatigue loading, details of which can be found in [15]. The calculation stems from an analysis of how residual stress affects the effective load ratio, R_{eff}, where the σ_{yy} term modifies the effective load ratio. The effective load ratio as a function of residual stress from the σ_{yy} term is shown in Figure 16. The σ_{xx} and σ_{zz} terms do not affect the FCGR for this case of loading in the *yy* direction.

Certainly, this behavior merits further investigation. It would be of interest if it can be deliberately induced by creating a constraint or toughness disparity between the weld metal and base metal

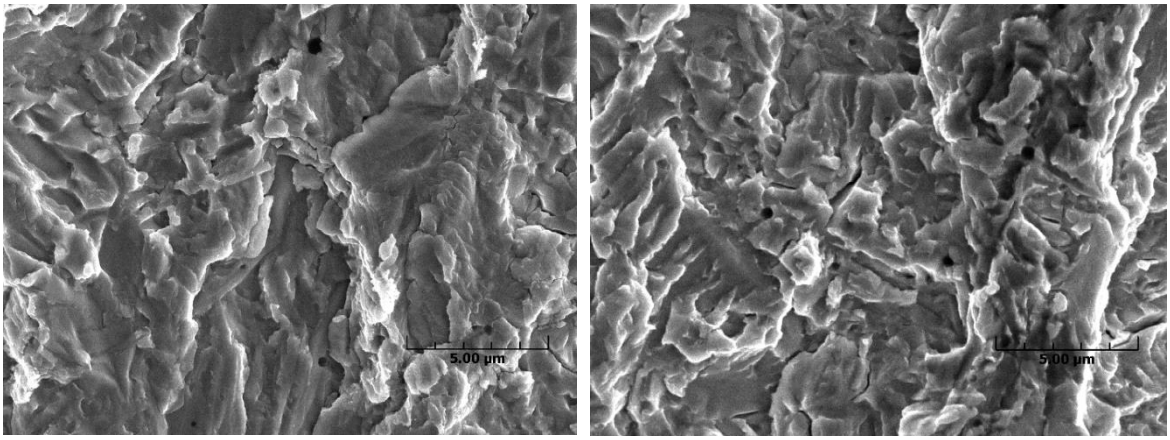

Figure 14. Fracture surfaces from the region of constant crack growth (flat FCGR, left) and rapid crack growth (right). Scale bar indicates 5 µm.

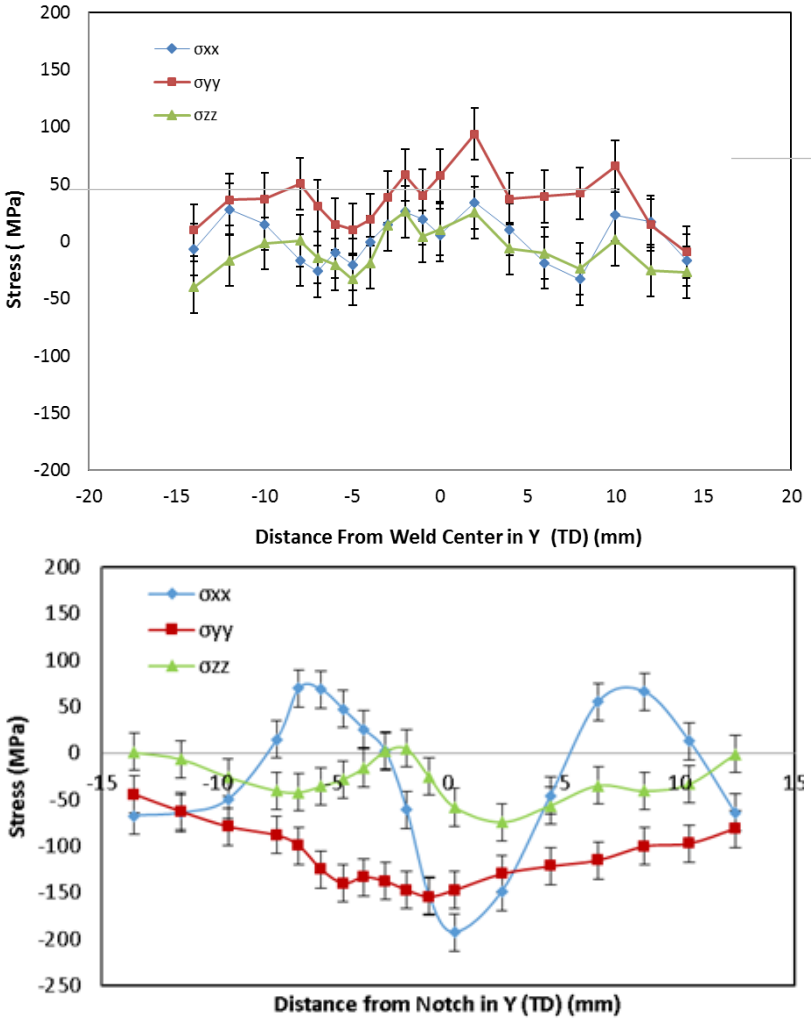

Figure 15. Residual stresses measured in CT specimens of girth welds from (top) the vintage X52 pipe and (bottom) the X70A pipe. Note that σ_{xx} is parallel to the crack-growth direction, σ_{yy} is perpendicular to the crack-growth direction, and σ_{zz} is in the through-thickness direction.

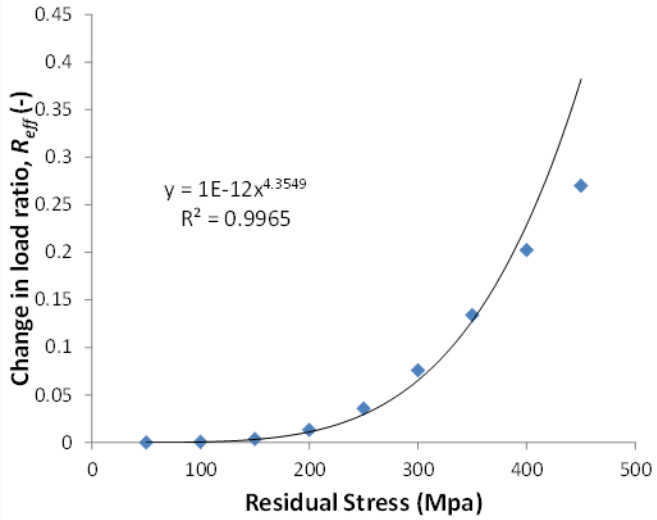

Figure 16. Calculated change in load ratio as a function of residual stress [15].

Related Work

Other work being performed that involves hydrogen effects on pipeline steels is being done under an agreement with the Department of Energy, Fuel Cells and Technologies Office. This work is being done in collaboration with Sandia National Laboratories, Livermore, CA, Oak Ridge National Laboratories, Oak Ridge, TN, and Colorado School of Mines, Golden, CO. The focus of the research is higher-strength pipeline steels and welds for future hydrogen applications. Higher strength steels can potentially provide cost benefits to pipeline operators and gas producers. An economic analysis of pipeline steels for application in hydrogen service can be found in the literature [20]. This research area includes mechanical measurements (Sandia National Laboratories), weld optimization, (Oak Ridge National Laboratories) and modeling (Colorado School of Mines) of X100 steels and welds.

Sandia National Laboratories has been conducting research on welds and HAZs of pipeline steels for the past few years [21, 22]. There has also been some work on X80 pipeline steel and its associated weld and HAZ in France [4]. This research involves pipeline steels with ferrite/pearlite microstructures, where the processing can yield a banded microstructure, which aids in lowering the diffusion of hydrogen to a crack tip, resulting in increased resistance to hydrogen-assisted fatigue crack growth.

Summary and Conclusions

The welds and HAZs from the four pipe sections tested exhibited hydrogen-assisted fatigue crack growth of the same order of magnitude as the base metal at both hydrogen gas pressures. There were no consistent trends seen, and there were no cases where the FCGR of a weld or HAZ was so much higher than that of the base metal, such as an increase in FCGR of more than 40%, which is approximately the uncertainty of the measurement method, that would raise concerns. The small variations that were observed were most often attributable to the microstructure through which the crack propagated. The constituents of the microstructure have a strong influence on the susceptibility of the FCGR. For example, the HAZ from the vintage X52 consistently exhibited a higher FCGR than the weld or base metal. The high carbon content resulted in the formation of martensite at the fusion line in the HAZ, and it is well-documented that untempered martensite can cause increases in hydrogen embrittlement [17, 23-25]. Care must be taken when designing hydrogen pipelines that the microstructural changes in the HAZ caused by welding can be controlled and are predictable. Further studies are needed to determine the microconstituents, grain sizes and orientation through which the crack traveled in the other materials to determine the role the microstructure played in those FCGRs.

Recommendations

Additional testing at a larger range of test parameters is necessary to determine the origins of some effects that are seen in the fatigue crack growth data. The regions of the FCGR curves that are flat tend to yield lower values of FCGR than those of base metal. More research into understanding the reason that this occurs would be helpful to industry, as this phenomenon could potentially be used to advantage in weld design. Another potential effect is that of residual stresses on welds and HAZs. Some recent measurements, in Connolly et al. [15] show that residual stresses of C(T) specimens cut from pipe sections are relatively small, but variations were seen from one pipe to another and understanding of the three-dimensional stress fields is incomplete.

A non-mandatory appendix, which contains the chemistries, tensile test results, images of weld microstructures and hardness maps, and results of fatigue crack growth tests to date, will be included in the ASME B31.12 code. In order to elevate the appendix to a mandatory status, additional FCGR tests on welds and HAZs at 34 MPa hydrogen gas pressure, and selected tests in air and at 21 MPa hydrogen gas pressure, in order to calibrate the model, will be needed. A simplified model for welds and HAZs, which uses multiple Paris Law coefficients, would be added at that time.

References

1. Chen, Y., Liu, M, Wang, Y-Y, Slifka, AJ, Drexler, ES, Amaro, RL, McColskey, JD, and Hayden, LE, *Performance evaluation of high-strength steel pipelines for high-pressure gaseous hydrogen transportation*. 2013: US Dept. of Transportation-PHMSA, DOT Project DTHP56-07-0001. p. 104.
2. Amaro, R.L., Findley, K. O., Rustagi, N., Drexler, E. S., Slifka, A. J., *Fatigue Crack growth of X100 Pipeline Steels in Gaseous Hydrogen.* International Journal of Fatigue, 2014. **59**: p. 262-271.
3. *ASME B31.12-2011, "Hydrogen Piping and Pipelines"*. 2012, American Society of Mechanical Engineers: New York, NY. p. 258.
4. Moro, I., Briottet, L., Lemoine, P., Doyen, O., and de Dinechin, G., *Fatigue crack growth of a C-Mn steel and associated weld under hydrogen pressure*, in *2012 International Hydrogen Conference, Hydrogen-Materials Interactions*, B.P. Somerday, and Sofronis, P., Editor. 2014, ASME Press: Moran, Wyoming. p. 309 - 317.
5. Holtam, C.M., and Baxter, D.P., *Fatigue performance of sour deepwater riser welds: crack growth vs. endurance*, in *ASME 2011 30th International Conference on Ocean, Offshore and Arctic Engineering*. 2011, ASME. p. 317 - 326.
6. Ronevich, J.S., and Somerday, B.P., *Measurement of fatigue crack growth relationships for steel pipeline welds in high-pressure hydrogen gas*, in *Steely Hydrogen 2014*, L. Duprez, Editor. 2014, OCAS: Ghent, Belgium. p. Session 12, Paper G09.
7. Thodla, R., Gordon, J.R., and Gui, F., *Effect of reeling on sour service fatigue crack growth behavior of welded API5L X65 line pipe.* Journal of Pressure Vessel Technology, 2015.
8. Wang, J., Li, X.Y., Zhang, Y.L., Miao, W., and Li, S.R., *Corrosion fatigue crack growth rates of X70 base metal and heat affected zone in H2S corrosive environment.* Corrosion Engineering, Science and Technology, 2015. **50**: p. 18 - 25.
9. Somerday, B.P. *III.5 Hydrogen Embrittlement of Structural Steels, Report No. SAND2014-16478R*. 2014 09/11/2015]; Available from: http://prod.sandia.gov/techlib/access-control.cgi/2014/1416478r.pdf.
10. DeArdo, A.J., Garcia, C.I., Palmiere, E.J., *ASM Handbook: Vol 4: Heat Treating*. 1991, ASM International: Materials Park, OH. p. 237-255.
11. Shikanai, N., Mitao, S. Endo, S., *Recent Development in Microstructural Control Technologies Through the Thermo-Mechanical Control Process (TMCP) with JFE Steel's High-Performance Plates*. 2008: JFE Technical Report No. 11, JFE Steel. p. 1-6.
12. Yuqun, Y., Yixin, H., Yongkuan, Y., Daoyuan, W., Yonglong, W., Stalheim, D.G. *Improved DWTT Performance on Heavy Gauge API Plate and Coil from 150 mm and 180 mm Thickness Slab at Nanjing Iron and Steel Company, Nanjing, China*. in *7th International Pipeline Conference*. 2008. Calgary, Alberta, Canada, IPC2008-64213.
13. *ASTM Standard E8/E8M-09 "Standard Test Method for Tension testing of Metallic Materials"*. 2009: West Conshohocken, PA.
14. *API SPEC 5L, "Specification for Line Pipe, Forty-fourth Edition"*. 2007, American Petroleum Institute: Washington, DC. p. 154.
15. *ASTM Standard E 647-11 "Test Method for Measurement of Fatigue Crack Growth Rates"*. 2011, ASTM International. p. 46.

16. Slifka, A.J., Drexler, E. S., Amaro, R. L., Lauria, D.S., Hayden, L.E., McCowan, C.N., and Sowards, J.W., *Measurements of fatigue crack growth rates of the heat-affected zones of welds of pipeline steels, Paper No. PVP2015-45242*, in *ASME 2015 Pressure Vessels and Piping Conference*. 2015: Boston, MA.
17. San Marchi, C., and Somerday, B.P. *Technical reference on hydrogen compatibility of materials: Plain carbon ferritic steels: C-Mn alloys (code 1100)*. 2010 October 2010 [cited 2012 January 3, 2012]; Available from: http://www.sandia.gov/matlsTechRef/.
18. Connolly, M.J., Amaro, R.L., Slifka, A.J., and Drexler, E.S., *Residual stresses in pipeline steel welds and their effect on pipeline lifetime predictions.* International Journal of Fatigue, in prep.
19. El-Soudani, S.M., and Pelloux, R.M., *Anisotopy of fatigue crack propagation in aluminum alloy butt welded joints.* Welding Research Supplement, 1975. **54**(May): p. 144s-152s.
20. Fekete, J.R., Sowards, J. W., Amaro, R. L., *Economic impact of applying high strength steels in hydrogen gas pipelines.* International Journal of Hydrogen Energy, 2015. **40**(33): p. 10547-10558.
21. Ronevich, J., and Somerday, BP. *Measurement of fatigue crack growth relationships for steel pipeline welds in high-pressure hydrogen gas*. in *Steely Hydrogen*. 2014. Ghent, Belgium.
22. Ronevich, J.A., B.P. Somerday, and C.W. San Marchi, *Effects of microstructure banding on hydrogen assisted fatigue crack growth in X65 pipeline steels.* International Journal of Fatigue, 2016. **82**: p. 497-504.
23. Walter, R., and Chandler, WT, *Influence of gaseous hydrogen on metal, Final Report*, p.f. NASA, Editor. 1973: Rocketdyne, Canoga Park, CA. p. 158.
24. Gangloff, R., Wei, R., *Gaseous hydrogen embrittlement of high strength steels.* Metallurgical and Materials Transactions A, 1977. **8**(7): p. 1043-1053.
25. Michler, T. and J. Naumann, *Microstructural aspects upon hydrogen environment embrittlement of various bcc steels.* International journal of hydrogen energy, 2010. **35**(2): p. 821-832.